

Role of ω -meson exchange in scaling of the $\gamma p \rightarrow \pi^0 p$ process from a Regge-type model with resonances

Kook-Jin Kong

Research Institute of Basic Sciences, Korea Aerospace University, Goyang, 412-791, Korea

Tae Keun Choi

Department of Physics, Yonsei University, Wonju, 26493, Korea

Byung-Geel Yu*

Research Institute of Basic Sciences, Korea Aerospace University, Goyang, 412-791, Korea

The scaling of photoproduction $\gamma p \rightarrow \pi^0 p$ is investigated in the Reggeized model with N^* and Δ resonances included to describe resonance peaks up to photon energy $E_\gamma = 3$ GeV. Given the t -channel exchanges $\rho(770) + \omega(780) + b_1(1235) + h_1(1170)$ Reggeized for the background contribution, the resonances of the Breit-Wigner form are introduced to agree with cross sections for total, differential and beam asymmetry in the low energy region. The scaled differential-cross sections $s^7 d\sigma/dt$ are reproduced to agree with the recent JLab data, revealing the production mechanism of the big bump structure around $W \approx 2.2$ GeV by the deep-dip pattern of the ω exchange that originates from the zeros of the trajectory $\alpha_\omega(t) = 0$ in the canonical phase, $\frac{1}{2}(-1 + e^{-i\pi\alpha_\omega(t)})$.

PACS numbers: 11.55.Jy, 13.75.Gx, 13.60.Le, 12.38.Lg

Keywords: scaling, scaled cross section, π^0 photoproduction, ω -meson, Regge model, Breit-Wigner resonance

By the modern theory of strong interaction hadrons consist of quarks and gluons and their interactions are governed by quantum chromodynamics. Due to the quark confinement, however, hadronic processes are observed in terms of meson and nucleon degrees of freedom. In this respect, it is of interest to search for evidences for quarks and gluon degrees of freedom shown up, in particular, in exclusive hadronic processes.

Recent experiments on pion photoproduction at JLab [1–3] have opened such a possibility by measuring the differential cross section at high energy and large momentum transfer which is predicted to obey the scaling, i.e.,

$$\frac{d\sigma}{dt} \sim F(t/s)s^{2-n}, \quad (1)$$

based on the quark-counting rule [4, 5]. Here n is the number of constituents (gauge boson plus the quarks) participating in the process. For the pion photoproduction, therefore, the measured cross sections in the CLAS glc collaboration are expected to show such a scaling behavior $s^7 d\sigma/dt \sim F(t_0/s) \sim \text{constant}$ at the fixed angle around $\theta = 90^\circ$ (or fixed t_0) as energy increases.

In this letter we investigate the process $\gamma p \rightarrow \pi^0 p$ with a focus on understanding the origin of the scaling at the level of hadronic degrees of freedom. As the existing data on this issue requires a model capable of reproducing not only the resonance peaks in the low energy but also the deep dip process observed at high energy it is advantageous to work with the reggeized model which includes nucleon resonances [6]. Since the Regge pole is in essence

a partial wave analytically continued to the complex angular momentum space, it is good to consider the nucleon resonance as the partial wave of the Breit-Wigner (BW) form for a specific angular momentum and parity eigenstate in the production amplitude.

In the neutral process where π^0 exchange is forbidden by charge-conjugation, $\omega(780)$, $\rho(770)$, $h_1(1170)$, and $b_1(1235)$ Regge poles are considered in the t -channel exchange to serve as a background contribution. Then, the whole amplitude will be composed of the t -channel Regge poles and the nucleon resonance R of spin- J possible to the process, i.e.,

$$\mathcal{M} = \mathcal{M}_{\text{Regge}} + \sum_{R=\Delta} \mathcal{M}_R^J + \sum_{R=N^*} \mathcal{M}_R^J. \quad (2)$$

We recall that the ω exchange with the phase $\frac{1}{2}(-1 + e^{-i\pi\alpha_\omega})$ and the ρ with $e^{-i\pi\alpha_\rho}$ are favored to describe the deep dip in the differential cross section in the reggeized model [7]. For a better agreement with the beam asymmetry Σ at high energy the exchanges of b_1 and the h_1 are further introduced with the constant phase taken [8]. In Table I the coupling constants and the Regge trajectories are summarized with the detailed expression for the $\mathcal{M}_{\text{Regge}}$ given in Ref. [8].

We now consider the resonances that are ranked as the four-star in Particle Data Group (PDG) for definiteness sake. For each resonance the partial wave is described by the helicity amplitude of Ref. [9] with the definition and the sign convention of the electric and magnetic multipoles further from Refs. [10, 11] in relation with the Chew, Goldberger, Low and Nambu (CGLN) amplitude.

* bgyu@kau.ac.kr

TABLE I. Coupling constants and trajectories for Regge poles. $g_{\gamma\pi V}$ is given in unit of GeV^{-1} .

meson	trajectory	phase	$g_{\gamma\pi V}$	g_{VNN}^v	g_{VNN}^t
ρ	$0.8t + 0.55$	$e^{-i\pi\alpha_\rho}$	0.255	2.6	16.12
ω	$0.9t + 0.44$	$\frac{-1+e^{-i\pi\alpha_\omega}}{2}$	0.723	15.6	0
b_1	$0.7(t - m_{b_1}^2) + 1$	1	0.189	0	-14
h_1	$0.7(t - m_{h_1}^2) + 1$	1	0.405	0	-14

Then, the resonance R of spin- J is written as

$$\mathcal{M}_R^J = \sum_{i=1}^4 H_i^J(W, \theta), \quad (3)$$

where the angular dependence of the amplitude H_i^J is expressed in the helicity formulation as in Ref. [9] with its energy-dependence given by the electric and magnetic multipoles [12],

$$E_{l\pm} = \frac{\beta_E}{\sqrt{q_R k_R j_\gamma(j_\gamma + 1)}} \frac{M_R \sqrt{\Gamma_{R\gamma N} \Gamma_{R\pi N}}}{M_R^2 - s - iM_R \Gamma} e^{-d\epsilon_R^2}, \quad (4)$$

$$M_{l\pm} = \frac{\beta_M}{\sqrt{q_R k_R j_\gamma(j_\gamma + 1)}} \frac{M_R \sqrt{\Gamma_{R\gamma N} \Gamma_{R\pi N}}}{M_R^2 - s - iM_R \Gamma} e^{-d\epsilon_R^2}, \quad (5)$$

respectively.

Note that the electromagnetic multipoles in Eqs. (4) and (5) are different from those in Ref. [12] in that the decay widths of resonance $R \rightarrow \gamma N$ and $R \rightarrow \pi N$ reported in the PDG are employed rather than Γ_E , Γ_M and $\Gamma_{l\pm}$ with cutoff parameters in Ref. [12] for less model-dependence. Instead, we use the β_E and β_M which are to be determined at the resonance position $W = M_R$ by using Eqs. (4) and (5). To be specific, $\beta_E(\beta_M)$ is determined by estimating $E_{l\pm}(M_{l\pm})$ and $\Gamma_{R\gamma N}$ in Eqs. (4) and (5) at $W = M_R$ from the following procedure [10]; Given the values of the helicity amplitudes $A_{1/2}$ and $A_{3/2}$ for $l+$ multipole amplitudes,

$$A_{1/2} = -\frac{1}{2} [(l+2)\mathcal{E}_{l+} + l\mathcal{M}_{l+}], \quad (6)$$

$$A_{3/2} = \frac{\sqrt{l(l+2)}}{2} [\mathcal{E}_{l+} - \mathcal{M}_{l+}], \quad (7)$$

and for $(l+1)-$ multipole amplitudes,

$$A_{1/2} = \frac{1}{2} [(l+2)\mathcal{M}_{(l+1)-} - l\mathcal{E}_{(l+1)-}], \quad (8)$$

$$A_{3/2} = -\frac{\sqrt{l(l+2)}}{2} [\mathcal{E}_{(l+1)-} + \mathcal{M}_{(l+1)-}], \quad (9)$$

where the multipoles $\mathcal{E}_{l\pm}(\mathcal{M}_{l\pm})$ are given by

$$a\mathcal{E}_{l\pm}(\mathcal{M}_{l\pm}) = \text{Im } E_{l\pm}(M_{l\pm}), \quad (10)$$

the $E_{l\pm}(M_{l\pm})$ can be estimated at $W = M_R$ with

$$a = C_I \left[\frac{1}{(2J+1)\pi} \frac{k_R}{q_R} \frac{M_N}{M_R} \frac{\beta_{\pi N}}{\Gamma} \right]^{1/2}, \quad (11)$$

$$C_{1/2} = -\sqrt{\frac{1}{3}}, \quad C_{3/2} = \sqrt{\frac{2}{3}}. \quad (12)$$

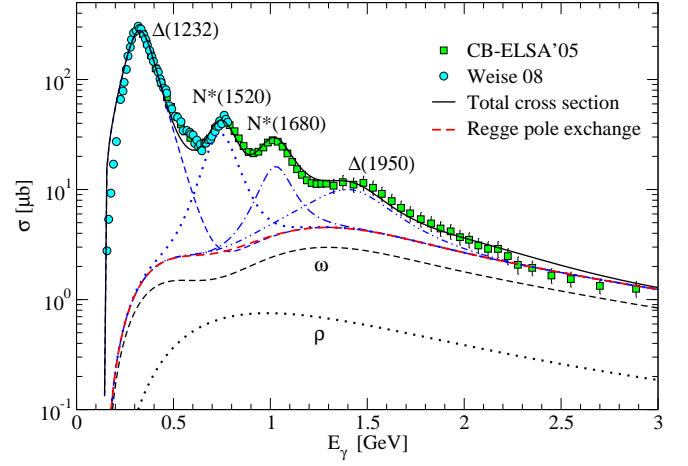


FIG. 1. (Color online) Total cross section for $\gamma p \rightarrow \pi^0 p$ from threshold to $E_\gamma = 3$ GeV. Red dashed line is the background from $\rho + \omega + b_1 + h_1$ Regge pole exchanges. Black solid line results from the background plus the resonances. Four resonances $\Delta(1232)$ (dashed), $N(1520)$ (dotted), $N(1680)$ (dash-dotted), and $\Delta(1950)$ (dash-dot-dotted) are illustrated to represent the sequential peaks. Data are taken from Refs. [3, 14].

Here $\beta_{\pi N}$ is the branching ratio of the resonance to the πN channel. Γ , M_R , J and I are the total width, mass, spin, isospin of the resonance R . k_R and q_R are momenta of photon and pion at the resonance position in the c.m. system. C_I is the Clebsch-Gordan coefficient and M_N is the nucleon mass.

With the known values for $A_{1/2}$ and $A_{3/2}$ the partial width $R \rightarrow \gamma N$ in Eqs. (4) and (5) is obtained as well from the equation,

$$\Gamma_{R\gamma N} = \frac{k_R^2}{\pi} \frac{2M_N}{(2J+1)M_R} [|A_{1/2}|^2 + |A_{3/2}|^2]. \quad (13)$$

In relation with Ref. [12], it is legitimate to write

$$\Gamma_{E(M)} \Gamma_{l\pm} = \beta_{E(M)}^2 \Gamma_{R\gamma N} \Gamma_{R\pi N}. \quad (14)$$

Then, the $\beta_E(\beta_M)$ estimated as discussed above, thus, provides the information about the case of coupling of the electric (magnetic) photon in the model of Ref. [12]. For a better description of the resonance we now introduce the cutoff factor $e^{-d\epsilon_R^2}$ to adjust the range of the resonance by a dimensionless parameter d together with the $\epsilon_R = \frac{M_R^2 - s}{M_R \Gamma}$ [13]. Therefore, there is no parameter, in essence, except for the d within the present framework where M_R , Γ , $\beta_{\pi N}$, and $A_{1/2}$ and $A_{3/2}$ are to be taken from PDG.

Before proceeding we wish to give a remark on the possibility of double-counting by the duality of the t -channel Regge poles to the s -channel resonances. The double counting should be considered in case when the contributions of the t -channel exchanges amount to an average of the resonance peaks in differential and, as a result, in total cross section [13]. It is expected that the negligence of it does not cause a serious problem in the

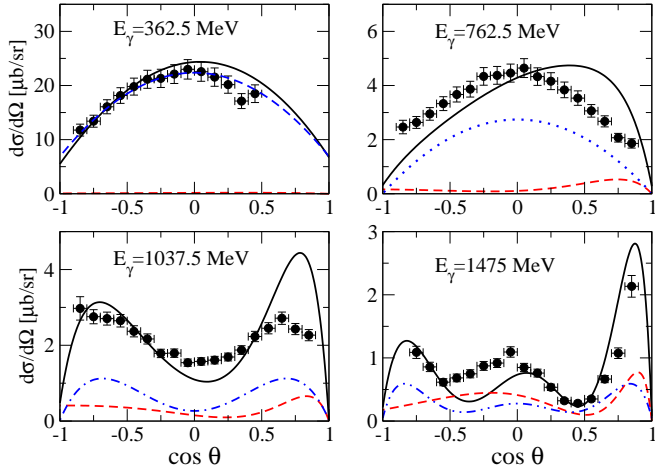


FIG. 2. (Color online) Differential cross sections for $\gamma p \rightarrow \pi^0 p$ in four energy bins $E_\gamma=362.5$ ($W=1249.2$), 762.5 (1520.3), 1037.5 (1681.5) and 1475 (1910) MeV. Data are taken from Ref. [3]. Notations for the curves are the same as in Fig. 1.

neutral pion case, however, because the contributions of the t -channel exchanges are not so much as those of the s -channel resonances to be taken an average, as can be seen in Figs. 1 and 2. Henceforth, we neglect the double-counting between the resonances and the Regge poles in the present calculation.

With the physical constants listed in table II which are within the range of PDG values, we present the total cross section in Fig. 1 up to $E_\gamma = 3$ GeV where the contributions of the resonances, $\Delta(1232)$, $N(1520)$, $N(1680)$, and $\Delta(1950)$ are shown to represent the four prominent peaks, respectively. The respective contributions of the ω and ρ Regge pole exchanges are illustrated by the dashed and dotted lines. In the Regge realm beyond $E_\gamma=3$ GeV, of course, the cross section coincides with that from the pure Regge pole exchanges as described in Ref. [8].

Figures 2 and 3 show the differential cross sections and the beam asymmetries reproduced at four energy bins each of which corresponds to the region around $\Delta(1232)$, $N(1520)$, $N(1680)$, and $\Delta(1950)$, respectively. The solid line is the total sum of the resonances and the t -channel Regge poles. The background contribution depicted by the red dashed line results from the t -channel Regge pole exchanges. The blue dashed, dotted, dashed-dot and dash-dot-dotted lines are from the $\Delta(1232)$, $N(1520)$, $N(1680)$, and $\Delta(1950)$ in order. These results are obtained through an optimal compromise between cross sections for total, differential, and beam asymmetry to agree with experimental data. Near the first resonance peak $W \approx 1232$ MeV, it is enough to consider $\Delta(1232)$ to describe the differential cross section and beam asymmetry. In the second resonance region mainly due to $N(1520)$, the resonances $N(1440)$ and $N(1535)$ are added to agree with the beam asymmetry Σ . To reproduce the differen-

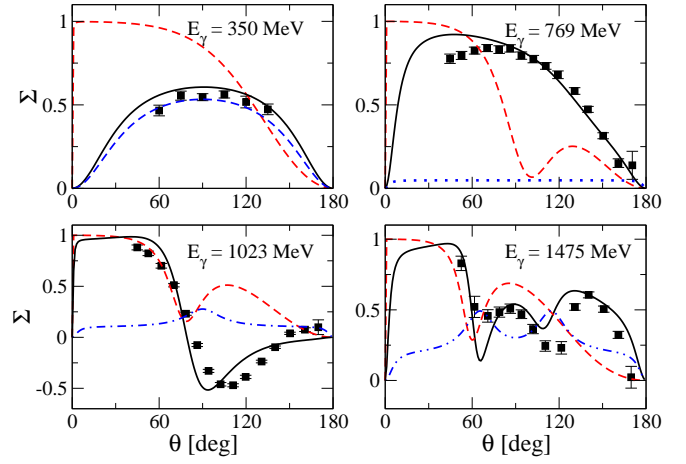


FIG. 3. Angular distribution of beam asymmetry Σ for $\gamma p \rightarrow \pi^0 p$ in four energy bins $E_\gamma=350$ ($W=1240$), 769 (1524), 1023 (1673) and 1475 (1910) MeV. Data are taken from Refs. [15, 16]. Notations for the curves are the same as in Fig. 1.

tial cross section at the third peak due to $N(1680)$, the resonance $\Delta(1700)$ together with $N(1650)$ play the role to fit to Σ . Around the fourth peak, apart from $\Delta(1950)$ which is a most representative one to cover this region, $\Delta(1910)$ is considered to give a further contribution to Σ .

Let us now discuss the feature of the differential cross section scaled by s^7 based on the framework we have established in the low energy region as well as at high energy. Figure 4 shows three scaled cross sections the first of which reproduces existing data at the angle $\theta = 90^\circ$, while the other two correspond to the cases at $\theta = 70^\circ$ and 50° , respectively. It is certain that the oscillatory behavior below $W \approx 2$ GeV is due to the resonances $\Delta(1232)$, $N(1520)$, and $N(1680)$ in order. Within

TABLE II. Physical constants for Δ and N^* resonances for $\gamma p \rightarrow \pi^0 p$. Widths and masses are given in unit of MeV, $A_{1/2}$, $A_{3/2}$ are given in unit of $\text{GeV}^{-1/2}$.

Resonance	J^P	M_R	Γ	$A_{1/2}$	$A_{3/2}$	$\beta_{\pi N}$	d
$\Delta(1232)$	$(3/2)^+$	1220	130	-0.13	-0.26	1.0	0.05
$N(1440)$	$(1/2)^+$	1400	190	-0.08	0.0	0.75	0.25
$N(1520)$	$(3/2)^-$	1505	120	-0.007	0.168	0.65	0.1
$N(1535)$	$(1/2)^-$	1515	150	0.13	0.0	0.55	0.25
$\Delta(1620)$	$(1/2)^-$	1590	120	0.055	0.0	0.3	0.25
$N(1650)$	$(1/2)^-$	1670	120	0.065	0.0	0.7	0.1
$N(1675)$	$(5/2)^-$	1660	135	0.01	0.015	0.35	0.2
$N(1680)$	$(5/2)^+$	1675	110	-0.01	0.10	0.675	0.1
$\Delta(1700)$	$(3/2)^-$	1675	250	0.12	0.12	0.15	0.25
$N(1720)$	$(3/2)^+$	1680	250	0.07	0.15	0.1	0.1
$\Delta(1905)$	$(5/2)^+$	1900	280	0.025	-0.04	0.1	0.2
$\Delta(1910)$	$(1/2)^+$	1885	220	0.06	0.0	0.3	0.25
$\Delta(1950)$	$(7/2)^+$	1890	240	-0.02	-0.10	0.35	0.1
$N(2190)$	$(7/2)^-$	2150	450	-0.065	0.035	0.1	0.2
$N(2220)$	$(9/2)^+$	2250	400	0.01	0.01	0.2	0.2
$N(2250)$	$(9/2)^-$	2275	500	0.01	0.01	0.1	0.2

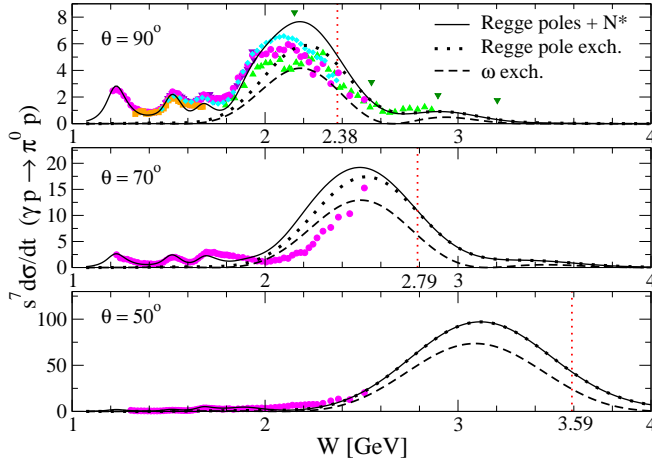


FIG. 4. (Color online) Scaled cross sections $s^7 \frac{d\sigma}{dt}$ ($10^7 \text{ GeV}^{14} \text{ nb/GeV}^2$) for $\gamma p \rightarrow \pi^0 p$ at $\theta = 90^\circ$, $\theta = 70^\circ$, and $\theta = 50^\circ$ as a function of total energy W . The scaled cross section agrees with data (green triangle-up) up to $W \approx 3$ GeV. N^* contributions vanish at $\theta = 50^\circ$. For the given angle θ the red dotted vertical line indicates the point of W corresponding to the upper limit of $t = -2 \text{ GeV}^2$ maximally allowed before saturation in Eq. (15). Data are taken from Refs. [2, 3, 15, 17–19].

the Regge framework where the production mechanism of the π^0 process is dominated by the ω exchange, the bump structure around $W \approx 2.2$ GeV, in essence, results from the deep-dip pattern that arises from the nonsense wrong signature zero (NWSZ) of the ω trajectory $\alpha_\omega(t) = 0$ [7, 8]. This in fact leads to the vanishing of the amplitude at $W \approx 1.58$ GeV at the angle $\theta = 90^\circ$, as shown in Fig. 4. While the cross section is suppressed in the low energy region, but amplified at high energy by the s^7 -power, the shift of the bump to the position $W \approx 2.5$ GeV at $\theta = 70^\circ$, and to 3.1 GeV at $\theta = 50^\circ$ in Fig. 4 can, thus, be understood as the result of a sequential shift of the NWSZ to $W \approx 1.75$ GeV, and to 2.11 GeV accompanying with the diffractive pattern according to the change of the angle. The resonance structures apparent in the scaled cross section at $\theta = 90^\circ$ vanish by degrees without affecting the structure of the bump as the angle becomes forward directional. This confirms our understanding of the production mechanism of the bump structure by the diffraction of ω within the present framework.

It is worth noting that the ρN cut plays a role in the scaled cross section for the cases of π^\pm processes [20]. In the π^0 case the ωN cut will be the corresponding one consisting of the amplitude $T_{\gamma p \rightarrow \omega p} T_{\omega p \rightarrow \pi^0 p}$. It may work in the present process as well with the b_1 -pole in the latter amplitude. Nevertheless we leave the estimate of the ωN cut behind because it is beyond the scope of the present work.

Before closing the discussion of the scaling, we must ask ourselves whether such an analysis of the present model is valid for the large angle, $\theta \approx 90^\circ$ in Fig. 4. The Regge theory is, in general, applied in the kinemat-

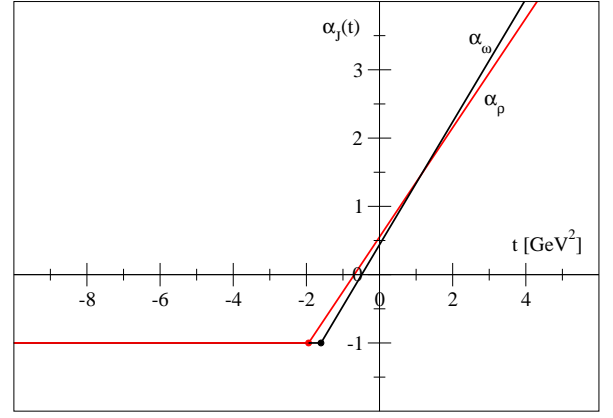


FIG. 5. (Color online) Saturation of the trajectory $\alpha(t) = \alpha_0 + \alpha' t$. The maximum ranges of t limited by $\alpha_i(t) > -1$ are $t > -1.94$ for ρ , $t > -1.6$ for ω , $t > -1.34$ for b_1 , and $t > -1.49 \text{ GeV}^2$ for h_1 , respectively.

cal region, $s \sim \text{large}$ and $t < 0$. Furthermore, in the large $-t$ limit the Regge trajectory is found to saturate [21]

$$\lim_{t \rightarrow -\infty} \alpha(t) \rightarrow -1, \quad (15)$$

as shown in Fig. 5. This puts a limit on the validity of the linear trajectory $\alpha(t) = \alpha_0 + \alpha' t$ in the Regge pole. For practical interest, here, we examine how far the range of energy W in the scaling could be accepted in accord with the point of t maximally allowed before saturation as in Eq. (15), i.e., at $-t = 2 \text{ GeV}^2$ from Fig. 5. The t -channel momentum transfer,

$$t = m_\pi^2 - 2k \left[\sqrt{q^2 + m_\pi^2} - q \cos \theta \right], \quad (16)$$

with this value at $\theta = 90^\circ$ leads to $W = 2.38 \text{ GeV}$, which could be an upper bound for the validity of the present analysis.

In summary, we have investigated the $\gamma p \rightarrow \pi^0 p$ process with a view to understanding the bump structure not expected from nucleon resonances but observed in the scaled cross section $s^7 d\sigma/dt$. It is pointed out that the big bump structure originates substantially from the dip-generation mechanism of the ω -meson exchange at the NWSZ in the scaled cross section within the present framework. For a reliable discussion on this issue we have proved an agreement with existing data on differential, total and the beam asymmetry, in particular, in the low energy region by including nucleon resonances basically without fit-parameters. Such resonance peaks in the scaled cross sections are reproduced well enough to confirm the validity of the scaling discussed in this work. The present approach will provide us a useful framework to analyze photoproduction data from threshold up to the energy region, coming of 12 GeV-upgrade at JLab for the forward angle, and to 3 GeV without the ωN cut for the intermediate angle where the scaled cross section is analyzed.

This work was supported by the grant NRF-2013R1A1A2010504 from National Research Foundation (NRF) of Korea.

-
- [1] L. Y. Zhu *et al.*, Phys. Rev. Lett. **91**, 022003 (2003); Phys. Rev. C **71**, 044603 (2005).
 - [2] M. Dugger *et al.*, Phys. Rev. C **76**, 025211 (2007).
 - [3] O. Bartholomy *et al.*, Phys. Rev. Lett. **94**, 012003 (2005).
 - [4] S. J. Brodsky and G. R. Farrar, Phys. Rev. Lett. **31**, 1153 (1973).
 - [5] G. P. Lepage, and S. J. Brodsky, Phys. Rev. D **22**, 2157 (1980).
 - [6] W.-T. Chiang, S. N. Yang, L. Tiator, M. Vanderhaeghen, and D. Drechsel, Phys. Rev. C **68**, 045202 (2003).
 - [7] M. Guidal, J.-M. Laget, and M. Vanderhaeghen, Nucl. Phys. A **627**, 645 (1997).
 - [8] B. G. Yu, T. K. Choi, and W. Kim, Phys. Rev. C **83**, 025208 (2011).
 - [9] R. L. Walker, Phys. Rev. **182**, 1729 (1969).
 - [10] I. G. Aznauryan, V. D. Burkert, and T.-S. H. Lee, arXiv:0810.0997.
 - [11] D. Drechsel, L. Tiator, J. Phys. G **18**, 449 (1992).
 - [12] H. Thom, Phys. Rev. **1510**, 1322 (1966).
 - [13] A. J. Lennox *et al.*, Phys. Rev. D **11**, 1777 (1975).
 - [14] M. Weis *et al.*, Eur. Phys. J. A **38**, 27 (2008).
 - [15] O. Bartalini *et al.*, Eur. Phys. J. A **26**, 399 (2005).
 - [16] A. A. Belyaev *et al.*, Nucl. Phys. B **213**, 201 (1883).
 - [17] M. A. Shupe *et al.*, Phys. Rev. D **19**, 1921 (1979).
 - [18] R. Alvarez *et al.*, Phys. Rev. Lett. **12**, 707 (1964).
 - [19] A. Imanishi *et al.*, Phys. Rev. Lett. **54**, 2497 (1985).
 - [20] J. M. Laget, Phys. Lett. B **685**, 146 (2010).
 - [21] R. Blankenbecler, S. J. Brodsky, J. F. Gunion, and R. Savit, Phys. Rev. D **8**, 4117 (1973).